ROYAL SOCIETY OF CHEMISTRY

PAPER

Check for updates

Mechanochemical one-pot synthesis and solid-state transformation of cobalt(II) Schiff base complexes: a green route to tailored coordination architecture

Hongguang Chen, Zhenwei Guo, [ID] Daming Feng, [ID] * Xudong Jin* and Fang Guo [ID] *

Schiff base complexes, traditionally synthesized *via* time-consuming, solvent-intensive solution methods, are pivotal in coordination chemistry but face limitations in accessing diverse architecture and sustainable scalability. Mechanochemistry has emerged as a solvent-free alternative, yet its potential to drive multicomponent reactions with precise control over metal–ligand coordination modes remains underexplored. Herein, we propose a mechanochemical one-pot synthesis strategy that synergistically integrates condensation, metal coordination, and deprotonation–dehalogenation reactions to fabricate Schiff base Co(II) complexes. Utilizing adamantylamine, 5-halosalicylaldehyde, and $CoCl_2 \cdot 6H_2O$ as precursors, mechanical forces drive the self-ordering of building blocks, enabling ultrahigh selective coordination and complex chemical processes. The approach efficiently yielded 12 Co(II) complexes, including the κ^1-*O*-monodentate **CoCl$_2$(HL)$_2$** and κ^2-*O*, *N*-bidentate **CoL$_2$**, which are typically challenging to access *via* conventional solution methods. Remarkably, the reactions achieved full conversion within 10 minutes, underscoring the rapidity and sustainability of mechanochemistry. Mechanical activation unlocked dormant reactivity in reactants, facilitating pathways otherwise inaccessible in solution. Furthermore, reversible solid-state transformations between complexes were demonstrated through dehydrohalogenation–hydrohalogenation processes. Specifically, **CoCl$_2$(HL)$_2$** is converted to **CoL$_2$** *via* cleavage of N–H and Co–Cl bonds and subsequent Co–N bond formation, while **CoL$_2$** reverts upon HCl absorption during grinding. This work highlights the utility of mechanochemistry in simplifying synthetic procedures, enhancing reaction complexity, and enabling green, solvent-free syntheses. By elucidating pathways for one-pot synthesis and solid-state transformations, it establishes mechanochemistry as a versatile and sustainable route for designing advanced coordination complexes with tailored architecture.

Introduction

The utilization of mechanical energy to induce or promote chemical transformations for driving chemical reactions has emerged as a significant approach in chemical synthesis.[1] This method notably reduces, or even entirely eliminates, the reliance on solvents, offering a more sustainable alternative to traditional solvent-based synthesis, and is progressively being recognized as an innovative green synthesis technique.[2,3] As a pivotal aspect of mechanochemical synthesis, grinding methods can effectively facilitate chemical reactions under solvent-free (NG) or liquid-assisted grinding (LAG) conditions.[4] These methods are particularly advantageous for reactions involving substances with poor solubility or substantial

discrepancies in solubility and have garnered considerable attention in the field of complex organic ligand preparation and their metal complexes.[5] Furthermore, grinding methods can alter established chemical reaction pathways and selectivity (yielding reaction pathways distinct from the thermodynamic products in solution),[6] thereby overcoming the constraints of traditional solution synthesis and allowing the formation of product structures that are challenging to generate or thermodynamically unfavorable in conventional solution methods, thus providing a potent tool for the discovery of new chemical reactivities, complex configurations, and transformation pathways.[7]

Schiff bases, characterized by their unique electronic properties, are capable of coordinating with various metal ions to form complexes with diverse geometries and stereo-selectivities,[8] an ability that positions them prominently in the field of coordination chemistry and demonstrates significant

College of Chemistry, Liaoning University, Shenyang 110036, China. E-mail: dmfeng@lnu.edu.cn; jinxudong@lnu.edu.cn; fguo@lnu.edu.cn

advantages in various fields,[9] including biomedicine,[10] photo-oxidation catalysis,[11] and chemical sensing.[12] However, traditional solution synthesis methods face numerous challenges in the preparation of Schiff bases and their corresponding complexes. Variations in the solubility of the reactants often require harsh conditions at high temperatures *via* thermodynamic control issues and low yields.[13] Furthermore, the imine bond is prone to hydrolysis or oxidation, which compromises the stability of Schiff bases, particularly in monodentate Schiff base complexes.[14] Mechanochemistry now facilitates the solvent-free synthesis of chelate complexes containing C=N ligands *via* mechanically driven imine condensation combined with *in situ* coordination, providing a rapid and environmentally friendly pathway to Schiff-base complexes.[15–17] Consequently, a significant area of research has developed, concentrating on the creation of novel Schiff-base complexes characterized by environmentally sustainable, controllable, and diverse structures, while also exploring the reversible solid-state conversion of their coordination configurations and their potential applications in biomedicine and other fields.[18] Nevertheless, a significant barrier to the advancement of structurally diverse coordination systems is the absence of strategies to concurrently manage multiple interrelated dynamic processes across various architectural factors, including reversible covalent bond formation, reversible hydrogen dehalogenation, and dynamic metal–ligand coordination.[19,20] Previous studies have documented hydrogen dehalogenation methods and the resultant changes in ligand structure before and after the reaction (Scheme 1a).[21] Notably, many Schiff base structures exhibit intramolecular bonding[22,23]

(Fig. S1), suggesting that dehydrohalogenation reactions may occur when reactants are appropriately oriented, potentially leading to the development of novel Schiff base complexes through structural transformations[24] (Scheme 1b).

In this context, it is essential to explore facile and atom-economical multicomponent reaction strategies that simultaneously modulate the dynamic interactions between hydrogen bonding sites, imine covalent sites, and coordination sites through mechanochemical one-pot methods, which aim to promote self-ordering behavior for the controllable preparation of Schiff complexes with various coordination modes. In particular, the construction of Schiff base bidentate and monodentate complex molecules exhibiting antimicrobial properties can be achieved using adamantyl compounds (*e.g.*, adamantanamine, adamantylethylamine, and memantine), which are employed in the treatment of influenza A virus, Parkinson's disease, and for the prevention of early influenza infections, as well as the treatment of severe Alzheimer's disease.[25,26] Furthermore, controlling the presence or absence of intracellular hydrogen bonding N–H–O is crucial for modulating cobalt(II) metal coordination modes in a controllable manner.

This study demonstrates that a series of monodentate Co(II) complexes, designated as **CoCl₂(HL)₂** (L = 2-((adamantan-1-yl)-imino-methyl)-4-chlorophenol and five additional ligand derivatives) can be synthesized through either sequential or one-pot mechanochemical synthesis *via* neat grinding of precursors A (amantadine, memantine, rimantadine), B (5-chloro-salicylaldehyde, 5-bromosalicylaldehyde) and CoCl₂·6H₂O in 2:2:1 molar ratio. These complexes are obtained quantitively
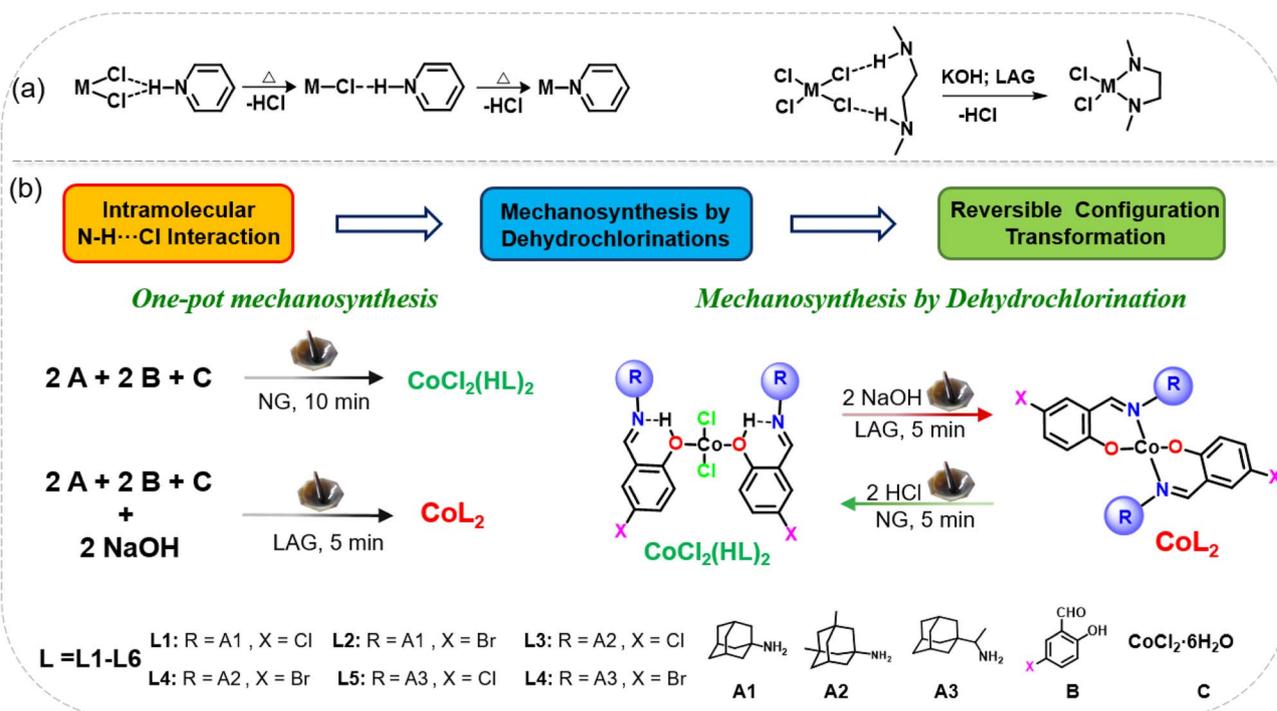
Scheme 1 Hydrodehalogenation methods have been reported (a). Mechanochemical one-pot process for the synthesis of **CoCl₂(HL)₂** and **CoL₂**, along with a reversible hydrogen dehalogenation scheme (b).

within 5 minutes under solvent-free conditions, as depicted in Scheme 1. By incorporating NaOH into the same reactant mixture and extending the grinding time to 10 minutes, a series of κ^2-O, N-bidentate **CoL$_2$** complexes can also be prepared using the same mechanochemical protocol. Mechanochemical dehydrochlorination of κ^1-O-monodentate **CoCl$_2$(HL)$_2$** enables the synthesis of κ^2-O, N-bidentate **CoL$_2$** complexes, while exposure to HCl allows reversible transformation of **CoL$_2$** back into κ^1-O-monodentate **CoCl$_2$(HL)$_2$**. Both transformations yield high purity products within 5 minutes. Notably, κ^1-O-monodentate **CoCl$_2$(HL)$_2$** complexes are challenging to synthesize and unstable in the solution, necessitating a solvent-free approach. This approach thus provides a novel pathway for preparing solvent-sensitive monodentate complexes.

Results and discussion

Six κ^1-O-monodentate **CoCl$_2$(HL)$_2$** complexes were synthesized through a one-pot mechanochemical process by mixing and grinding component A (adamantanamine, adamantylethyl-amine, and memantine), component B (5-chlorosalicylaldehyde and 5-bromosalicylaldehyde), and component C (CoCl$_2$·6H$_2$O) in a molar ratio of 2:2:1 over a duration of 10 minutes, resulting in a green powder. Grinding under the same reaction conditions and utilizing the same reactant system with the addition of 2 equivalents of NaOH resulted in the formation of six distinct κ^2-O, N-bidentate complexes **CoL$_2$**, characterized by a red powder that differed from the previously observed κ^1-O-monodentate complexes, which were formed alongside NaCl, as confirmed by the presence of entirely new diffraction peaks in the powder X-ray diffraction (PXRD) pattern shown in Fig. 1 and S2, S3. The analysis of the PXRD patterns of the synthesized

products revealed that the diffraction peak positions and intensities of the ground products closely matched those of the crystal simulations and the Schiff base cobalt complex reported in the literature. This strongly confirms the success of the mechanochemical multicomponent one-pot method for synthesizing the metal–organic complexes, thereby demonstrating the feasibility and validity of this synthesis strategy within this system. The PXRD patterns of the remaining five pairs of complexes are presented in Fig. S4–S8. FT-IR analysis reveals that hydrogen-bond-mediated κ^1-O-monodentate **CoCl$_2$(HL)$_2$** exhibits a loss of O–H at 3430 cm^{-1} and N–H at 3220 cm^{-1}, in contrast to the dehydrochlorination process yielding κ^2-O, N-bidentate **CoL$_2$**, which shows a red-shifted C=N at 1600 cm^{-1} and a new Co–N bond at 480 cm^{-1} (Fig. S25–S36). High-resolution mass spectrometry (HRMS-ESI) tests indicate that the experimental values are consistent with their theoretical values, demonstrating that the structure of the complexes synthesized *via* mechanochemical one-pot methods corresponds to the structures obtained through quantitative synthesis. In summary, mechanochemistry can efficiently and controllably synthesize κ^1-O-mono- and κ^2-O, N-bidentate cobalt Schiff base complexes.

Among all possible combinations of initial components, if further condensation of an imine-containing ligand can provide an optimal coordination environment for the metal, the formation of this ligand can be selectively facilitated by its preferential binding to the transition metal, allowing for the formation of complexes with different configurations selectively.[27] During the one-pot synthesis, the condensation covalent reaction of ammonia and aldehyde, the metal coordination reaction, and the deprotonated dehalogenation reaction were allowed to take place in the same reaction system
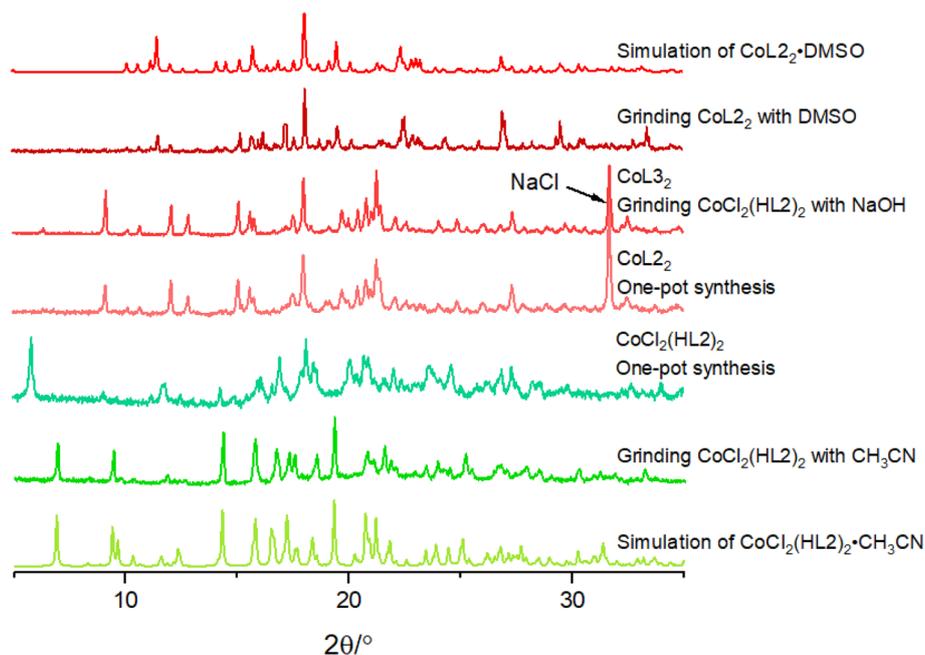

Fig. 1 PXRD patterns of κ^1-O-monodentate **CoCl$_2$(HL2)$_2$** complexes and κ^2-O, N-bidentate complexes **CoL2$_2$** synthesized by a mechanochemical one-pot process and dehalogenation of hydrogen.

synergistically; the reaction system underwent synergistic and complex chemical processes facilitated by mechanical force, inducing self-classification and ultra-high-selective coordination, successfully realizing the highly efficient construction of cobalt metal–organic complexes. The mechanochemical synthesis of Schiff base ligands and their cobalt κ^1-O-mono- and κ^2-O, N-bidentate complexes can be fully achieved after 10 minutes, and this study highlights the feasibility of mechanochemistry in the sustainable synthesis of complex organic ligands and their metal complexes. Compared to the solution method, the mechanochemical one-pot synthesis has advantages such as solvent-free conditions, rapid processing, minimal energy consumption, and by-products consisting solely of NaCl, as detailed in Table S5. More importantly, the UV spectra of the monodentate complexes in six common organic solvents reveal that, in addition to the peak at 325 nm, a new red-shifted absorption peak appears at 390 nm in organic protic solvents, compared to the characteristic absorption peaks in non-protic solvents (Fig. S37–S42). This indicates a change in the coordination mode of the complex in protic solvents, suggesting rapid dehydrochlorination and coordination rearrangement. Therefore, mechanochemical methods can synthesize monodentate cobalt complexes that are not achievable through conventional solution methods.

The above ground product can be readily crystallized using appropriate solvents, giving rise to crystals for X-ray single crystal structural determination. As illustrated in Tables S1 and S2, the formation of the two lattices is contingent upon the adamantanamine/memantine and adamantane ethylamine ligands, where the presence or absence of methylene groups in proximity to the reaction site of the amino molecule is crucial for the lattice formation. The crystals of the methylene-free κ^1-O-monodentate complexes formed from the Schiff base ligands L1–L4, derived from amantadine and memantine, are labeled as **CoCl₂(HL1)₂·CH₃CN**, **CoCl₂(HL2)₂·CH₃CN**, **CoCl₂(HL3)₂**, and **CoCl₂(HL4)₂**, respectively, and exhibit isostructures belonging to the space group $P2_1/c$ (see Table S1). Notably, powder X-ray diffraction patterns reveal significant differences between **CoCl₂(HL1)₂·CH₃CN**, **CoCl₂(HL2)₂·CH₃CN** and **CoCl₂(HL3)₂**, **CoCl₂(HL4)₂**, indicating that structural rearrangements occurred with solvent participation (Fig. 2 and S9). Conversely, the adamantylethylamine κ^1-O-monodentate complexes **CoCl₂(HL5)₂** and **CoCl₂(HL6)₂**, which contain methylene groups, share the same space group $C2/c$.

Herein, we utilize **CoCl₂(HL2)₂·CH₃CN** as a representative example to describe the crystal structures of κ^1-O-monodentate Schiff base complexes formed by ligands L1–L4. The crystal crystallizes in the monoclinic $P2_1/c$ space group, with one asymmetric unit consisting of a **CoCl₂(HL2)₂** and one acetonitrile molecule. As seen in Fig. 3, the cobalt ion coordinates with two singly adjacent protonated HL molecules and two chlorine ions simultaneously, forming a four-coordinated configuration with an irregular tetrahedral spatial geometry ($\tau_4 = 0.8998$), where each HL acts as a κ^1-O-monodentate coordination site via its phenolic oxygen atoms. The corresponding Co–O and Co–Cl bond lengths are 1.9610 Å (Co–O1) and 1.9530 Å (Co–O2), 2.2280 Å (Co–Cl1) and 2.2807 Å (Co–Cl2), the two hydroxyl groups form
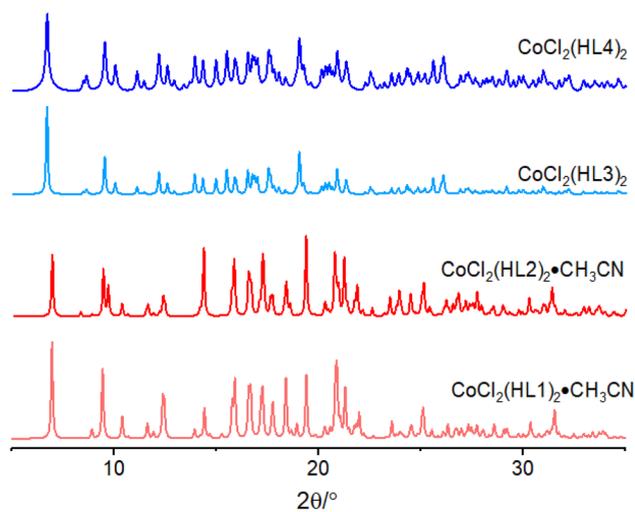

Fig. 2 PXRD spectra of crystals of **CoCl₂(HL1)₂·CH₃CN**, **CoCl₂(HL2)₂·CH₃CN**, **CoCl₂(HL3)₂** and **CoCl₂(HL4)₂** obtained by recrystallisation.

coordination dihedral angles of 81.26°. The C=N bond maintains the planarity with the bromosalicylaldehyde ring, with the dihedral angle of 8.00° and 3.09°. The protonated hydroxyl forms intramolecular N–H···O hydrogen bonds (1.982 Å, 1.900 Å) with the N of imine, which commonly exists in most Schiff ligands. The **CoCl₂(HL)₂** units are connected with each other through extensive C–H···Cl and C–H···Br hydrogen bonding, and the included acetonitrile molecule is linked with the **CoCl₂(HL)₂** unit via weak C–H···N and C–H···Cl interactions to maintain the stability of the structure (Fig. S10). The coordination and stacking patterns of **CoCl₂(HL1)₂·CH₃CN** and **CoCl₂(HL2)₂·CH₃CN** are identical (Fig. S11). Both **CoCl₂(HL3)₂** and **CoCl₂(HL4)₂** exhibit identical coordination patterns and involve robust intramolecular hydrogen bonds between the imino nitrogen and the phenolic oxygen, resulting in the formation of an additional six-membered ring (Fig. S12). The structures are more tightly stacked as the asymmetric unit does not contain solvent molecules.

The κ^1-O-monodentate complex crystals formed by the adamantylethane Schiff base ligands L5 and L6 are labeled **CoCl₂(HL5)₂** and **CoCl₂(HL6)₂**, respectively. These complexes are isostructural, sharing the same space group $C2/c$, with each asymmetric unit containing half of a complex molecule and exhibiting similar unit cell parameters, as shown in Table S2. In the crystal, the cobalt ions form a four-coordination configuration characterized by irregular tetrahedra ($\tau_4 = 0.89$), involving two individual protonated HL molecules and two chloride ions Fig. 4. Notably, the two C=N bonds remain approximately planar with bromosalicylaldehyde; however, the distance between the two nitrogen atoms is 8.02 Å. The two hydroxyl groups create coordination dihedral angles of 69.09° and 80.98°. Furthermore, two intramolecular N–H···O hydrogen bonds are formed, with bond lengths of 1.948 Å and 1.955 Å. The neighboring complex molecules are primarily interconnected through C–H···Cl weak interactions, resulting in

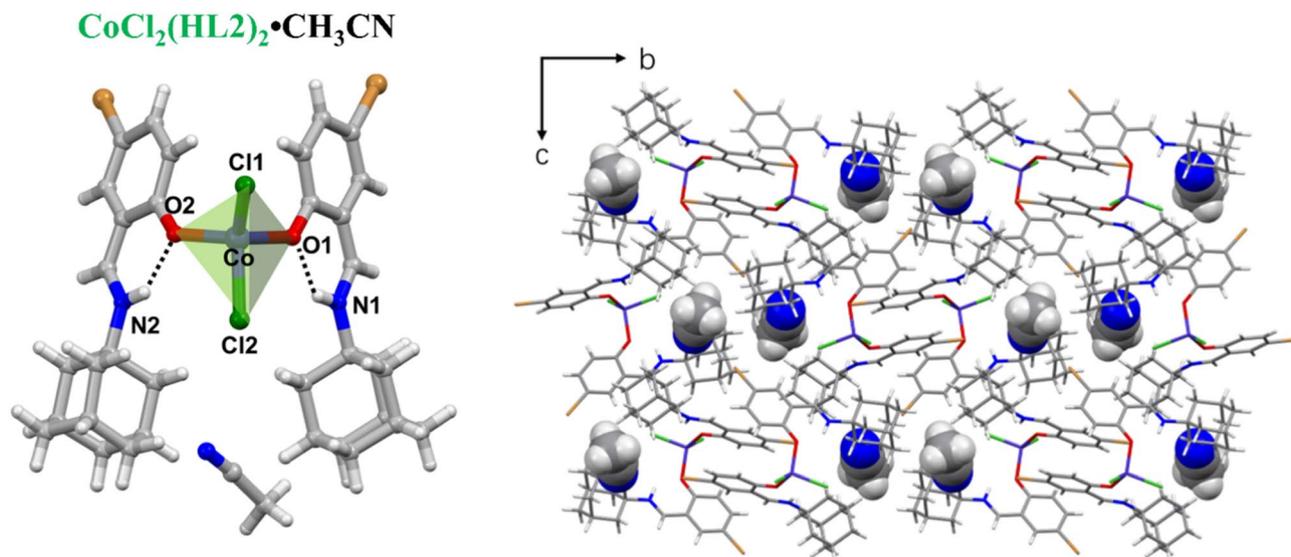**Fig. 3** Crystal structure and their packing for **CoCl$_2$(HL2)$_2$**.

chain stacking along the C-axis direction, which facilitates the maintenance of a relatively stable position and orientation within the crystal (Fig. S13).

The product formed mechanochemically by dehydrochlorination was further recrystallized from solvents, giving rise to crystals suitable for single crystal X-ray diffraction, and the product was labelled **CoL$_2$** (L = L1–L6), respectively. As illustrated in Table S3, the presence or absence of methylene in the neighbourhood of the amino covalent reaction site also influences the lattice formation of κ^2-O, N-bidentate complexes. The methylene-free κ^2-O, N-bidentate complex crystals formed by ligands L1, L3 and L4 show an isomorphic structure belonging to the *Pbca* space group. In contrast, **CoL2$_2$·DMSO**, which includes the solvent molecule DMSO, belongs to the $P\bar{1}$ space group. Conversely, the κ^2-O, N-bidentate complexes **CoL5$_2$** and

CoL6$_2$, derived from the methylene-containing ligands L5 and L6, share the same $P2_1/c$ space group. It is noteworthy that **CoL2$_2$·DMSO** has the same space group as the previously reported **CoL2$_2$·EtOH**; although with different cell parameters, it is considered to be a pseudo-polycrystalline form of **CoL2$_2$**.[28] The DMSO solvent molecules are released upon heating (Fig. S14) and can also be recovered through LAG grinding; PXRD diffraction (Fig. S15) confirms the significant changes in the lattice structure.

Here we describe the crystal structures of κ^2-O, N-bidentate Schiff base complexes formed from the ligands L1–L4 using **CoL2$_2$·DMSO** as a representative. **CoL2$_2$·DMSO** crystallizes in the triclinic $P\bar{1}$ space group, with one asymmetric unit consisting of one **CoL2$_2$** and one dimethyl sulfoxide molecule, as seen in Fig. 5. Although the cobalt ion maintains a four-
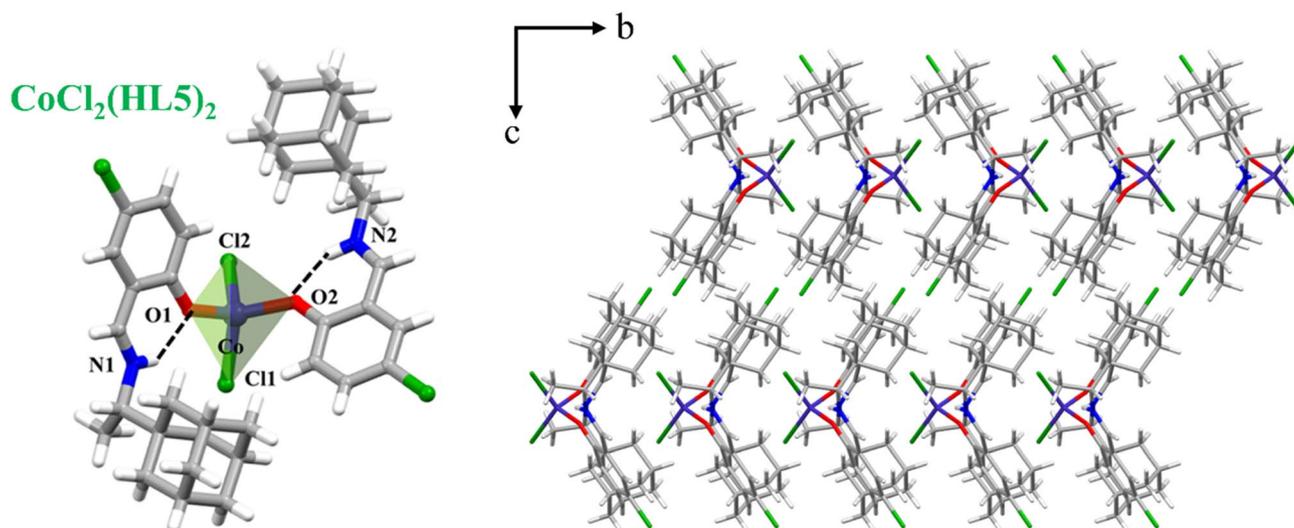

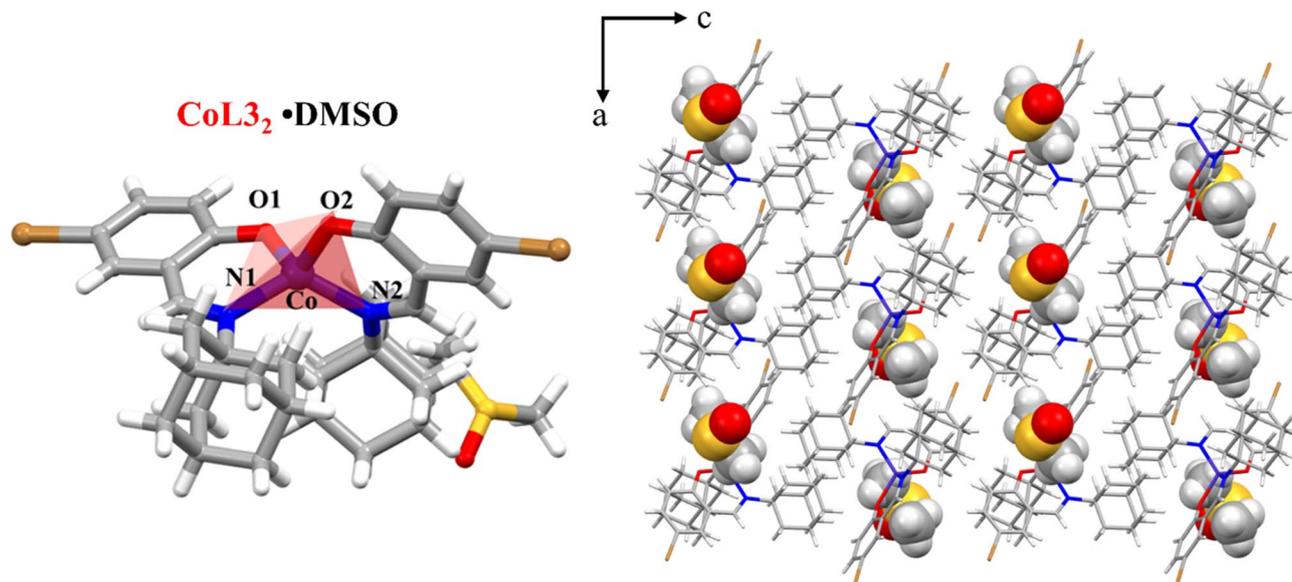**Fig. 4** Crystal structure and their packing for **CoCl$_2$(HL5)$_2$**.

Fig. 5 Crystal structure and packing for **CoL3$_2$·DMSO**.

coordination structure with an irregular tetrahedral spatial geometry ($\tau_4 = 0.8500$), the Co ion coordinates with phenolic O atoms (O1 and O2) and imine N atoms (N1 and N2) of two singly deprotonated ligands simultaneously to form two nearly planar six-membered rings. The corresponding bond lengths of Co–N and Co–O are 1.9930 Å (Co–N1) and 2.0030 Å (Co–N2), 1.9606 Å (Co–O1) and 1.9130 Å (Co–O2). There are two types of O–Co–N bond angles. Some are smaller than 109.5° for an ideal tetrahedron, while the others are wider. All bond angles of O–Co–O (112.90°) and N–Co–N (123.14°) are larger than 109.5°. The dihedral angle between the two chelate planes formed by Co–N–C–C–C–O is 86.76°, indicating that the two chelate planes are almost perpendicular. The **CoL2$_2$** unit is connected with each other through extensive C–H···Br hydrogen bonding. The included DMSO molecule is connected with the **CoL2$_2$** unit *via* C–H···O weak interactions to retain the stability of the structure (Fig. S16). **CoL1$_2$**, **CoL3$_2$**, and **CoL4$_2$** exhibit the same cobalt bonding modes and coordination configurations as **CoL2$_2$-DMSO**, with the exception of the solvent-free molecules (Fig. S17). All κ^2-*O*, *N*-bidentate coordination modes of the complexes do not involve intramolecular hydrogen bonds because the ligand has been deprotonated, but there also exist two six-membered rings through a cobalt ion, two oxygen atoms and two nitrogen atoms.

The κ^2-*O*, *N*-bidentate complexes **CoL5$_2$** and **CoL6$_2$** crystallize in the monoclinic system, belonging to the $P2_1/c$ space group, each asymmetric unit comprises one cobalt(II) complex. The central cobalt(II) in both **CoL5$_2$** and **CoL6$_2$** lies on a twofold rotation axis and is bonded to the oxygen and nitrogen donors of the two κ^2-*O*, *N*-bidentate ligands in a *trans* arrangement (Fig. 6 and S18).[29] The complexes exhibit a distorted tetrahedral geometry ($\tau_4 = 0.83$), as the τ_4 parameter is less than 0.85, indicating a configuration that is more distorted than that of other κ^2-*O*, *N*-bidentate complexes. The dihedral angle between

the two coordination planes defined by O1–Co1–N1 and O2–Co1–N2 measures 86.01° for **CoL5$_2$** and 85.76° for **CoL6$_2$**. Additionally, the relatively large distance between the adamantylethylamine cages of the two ligands leads to an anticoordination phenomenon, where the imine-coordinated form predominates. The κ^2-*O*, *N*-bidentate coordination inhibits the formation of intramolecular hydrogen bonds due to the deprotonated ligands; however, two six-membered rings are also present, formed through a cobalt ion, two oxygen atoms, and two nitrogen atoms in both **CoL5$_2$** and **CoL6$_2$**.

The crystal structure reveals that the conversion of κ^1-*O*-monodentate complexes to κ^2-*O*, *N*-bidentate complexes occurs through dehydrochlorination, accompanied by a reduction in the distance between the metal and the ligand. This process facilitates the 'squeezing' of ligands, resulting in a more tightly packed κ^2-*O*, *N*-bidentate coordination configuration. The inherent instability of κ^1-*O*-monodentate molecules, which are loosely packed due to longer coordination bonds compared to κ^2-*O*, *N*-bidentate complexes, is further exacerbated by dehydrogenation stemming from the disruption of intramolecular hydrogen bonds. This dehydrogenation serves as the primary driving force for the transition from κ^1-*O*-monodentate to κ^2-*O*, *N*-bidentate coordination. Even in the absence of alkaline substances, hydrogen bonding can still occur in protonic solvents such as methanol and ethanol, which contain both hydrogen bond donors and acceptors. This interaction disrupts the N–H···O intramolecular hydrogen bonding, resulting in a rearrangement of the coordination mode that diminishes the selectivity for κ^1-*O*-monodentate complexes, ultimately leading to the exclusive formation of κ^2-*O*, *N*-bidentate complexes. Moreover, during this rearrangement process, the metal cation does not form a coordination bond with solvent molecules; instead, it acts as a strong hydrogen bond acceptor, facilitating the removal of the halogen anion and stabilizing the
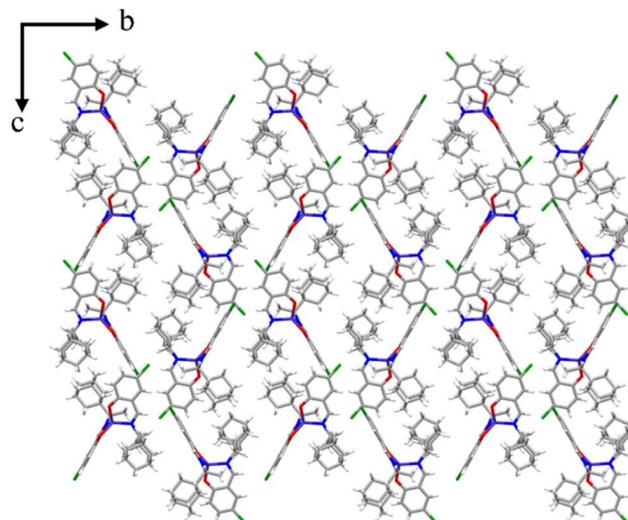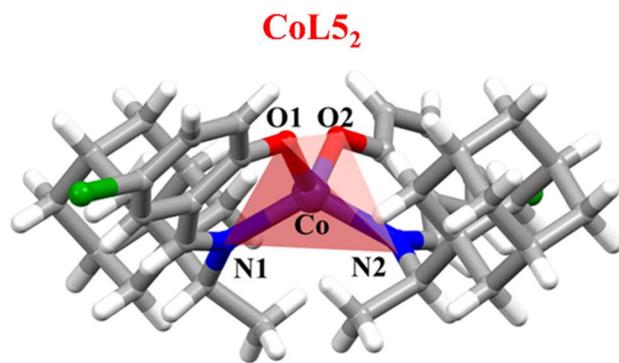
Fig. 6 Crystal structure and packing for **CoL5₂**.

coordination rearrangement. The κ^1-*O*-monodentate complexes yielded single crystals with κ^2-*O*, *N*-bidentate coordination, except when recrystallized in acetonitrile solvent, thereby validating our design principle. In contrast, conventional solvothermal synthesis typically incorporates nitrogen and oxygen into their coordination spheres, resulting in the formation of only a single κ^2-*O*, *N*-bidentate coordination.[30,31] This paper presents a solvent-free one-pot mechanochemical synthesis that mitigates the influence of solvents, thereby accelerating the formation of κ^1-*O*-monodentate coordination and preventing its rearrangement, allowing the synthesis of κ^1-*O*-monodentate complexes that cannot be achieved by solvent methods. Additionally, κ^2-*O*, *N*-bidentate complexes can be further synthesized through alkali grinding and dehalogenation of hydrogen, and the selective preparation of κ^1-*O*-monodentate and κ^2-*O*, *N*-bidentate coordination structures is facilitated by utilizing intramolecular hydrogen bonding to regulate the self-sorting process of mono- and κ^2-*O*, *N*-bidentate coordination.

Factors such as the denticity, electronic properties and steric site resistance of the ligand can modulate its binding strength to transition metals, which results from the unique electronic configuration of the ligand that imparts a specific coordination tendency to the transition metal.[19,32] When the initial organic component, adamantanamine, is replaced by the more electron-donating adamantylethylamine and memantine, or when the 4-substituent of salicylaldehyde is altered from chlorine to bromine, the resulting κ^1-*O*-monodentate and corresponding κ^2-*O*, *N*-bidentate complexes do not exhibit significant changes in the coordination conformations of cobalt and the ligand, suggesting that remote electronic interactions do not substantially affect the binding between the metal and the ligand site. However, from the perspective of crystal stacking, the volume of the amino group significantly influences the crystal arrangement. The larger volumes of adamantylethylamine and memantine occupy the voids during molecular stacking, displacing solvent molecules in the crystal structure of

the smaller volume adamantyl Schiff base complexes. Additionally, the spatial site resistance attributed to the positional isomerism of adamantylethylamine and memantine near the coordination site does not alter the coordination denticity between the metal and the ligand, but it does affect the coordination conformation of the Co(II) and Schiff base κ^1-*O*-monodentate complexes. In this context, the greater spatial site resistance of adamantylethylamine leads to a *trans*-coordination of the two Schiff base ligands, resulting in a distinct stacking pattern.

Reversible solid-state conversion between κ^1-*O*-monodentate and κ^2-*O*, *N*-bidentate complexes. The solid-state transformation was carried out by adding an appropriate ratio of base using complexes **CoCl₂(HL)₂** (L = L1–L6) as the starting materials, respectively. As seen in Fig. 7, by grinding complexes **CoCl₂(HL)₂** and the strong base NaOH in the molar ratio of 1 : 2 in the presence of two drops of methanol (60 µL), a color change from green to red was visible within 5 minutes, indicating the

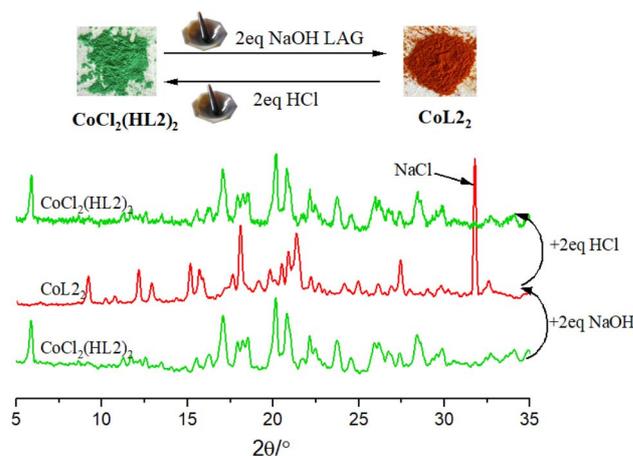Fig. 7 Solid-state transformation of **CoCl₂(HL2)₂** into **CoL2₂** by adding an appropriate ratio of base.

generation of a new phase. PXRD analysis confirmed that the red sample obtained after grinding was the κ^2-O, N-bidentate complex **CoL$_2$**. The release of HCl was corroborated by the presence of NaCl ($2\theta = 31.5°$) which was formed as a byproduct. In addition, the red **CoL$_2$** (L = L1–L6) solid, when ground with equimolar hydrochloric acid, undergoes a reverse reaction in the solid state, involving molecular rearrangement facilitated by the re-addition of HCl molecules to the structure, resulting in the production of the green complex **CoCl$_2$(HL)$_2$**, which is further corroborated by PXRD (Fig. S19). The application of mechanical force during the re-addition halogenation provides a novel synthetic route to the Schiff base cobalt κ^1-O-monodentate complexes, which cannot be synthesized through conventional solution methods. It is noteworthy that the direct grinding conversion of **CoCl$_2$(HL1)$_2$·CH$_3$CN** to **CoCl$_2$(HL3)$_2$·DMSO** could not be achieved due to the encapsulation of different solvent molecules in the solvated crystalline phase, and a solid powder could not be obtained directly when utilizing DMSO as the LAG medium, attributed to its excellent solvation properties. Therefore, we employed both unsolvated **CoCl$_2$(HL1)$_2$** and **CoCl$_2$(HL3)$_2$** to modulate the dehalogenation process by disrupting the intramolecular hydrogen bonding, facilitating the transformation from κ^1-O-monodentate into κ^2-O, N-bidentate coordination. Other corresponding mono- and bi-dentate complexes can also undergo reversible dehalogenation and hydrogen conversion reactions, a process that has been confirmed by PXRD, as shown in Fig. S20–S24.

In the dehydrochlorination reaction, the potential intramolecular charge assisted N–H(+)···Cl(−) interactions in **CoCl$_2$(HL)$_2$** cause hydrogen and coordination bonds to break and release H and Cl upon mechanochemical grinding with NaOH and then formation of the coordination bond of Co–N occurs to give **CoL$_2$**. Thus, with proper orientation and plausible N–H(+)···Cl(−) interactions, it is assumed that the dehydrochlorination reaction that uses charge assisted N–H(+)···Cl(−) interactions can be applied to the precision synthesis of other similar Schiff base complexes. Under the influence of mechanical force, the addition of HCl leads to the protonation and subsequent breakdown of the Co–N coordination bond involving the nitrogen atom, which facilitates the formation of a new coordination bond between Cl and Co. Additionally, the stability of the six-membered ring structure allows for the recovery of the N–H···O intramolecular hydrogen bonding interactions, resulting in the successful preparation of Schiff base κ^1-O-monodentate complexes.

Antibacterial activity

Schiff base κ^1-O-monodentate and κ^2-O, N-bidentate complexes were used to test against one Gram-positive (*Bacillus subtilis*) and one-Gram negative bacteria (*Escherichia coli*) by the zone of inhibition method. The samples were prepared at concentrations of 1.0×10^{-1}, 1.0×10^{-2}, 1.0×10^{-3} and 1.0×10^{-4} mol L^{-1} in DMF. The diameters of growth inhibition zones were measured after 48 h and the results are presented in Table S4 and Fig. S43, S44. Under the same conditions, κ^1-O-monodentate and κ^2-O, N-bidentate complexes showed better antibacterial effects against two bacteria compared with HL, which indicated that the

biological activity of the Schiff base ligand improved after coordination with metallic Co. Furthermore, the antibacterial effects of the two complexes were significantly concentration-dependent; as the concentration increased, the diameters of the bacterial inhibition zones also increased, demonstrating enhanced antibacterial activity. Notably, the κ^1-O-monodentate complexes **CoCl$_2$(HL3)$_2$** and **CoCl$_2$(HL4)$_2$**, which contain memantine, exhibited the highest antimicrobial activity against *Escherichia coli*, with inhibition zone diameters of 18.0 mm and 20.0 mm, respectively, at a concentration of 1.0×10^{-1} mol L^{-1} (Fig. 5). In contrast, the κ^2-O, N-bidentate complexes containing chlorosalicylaldehyde demonstrated superior antibacterial activity against *Bacillus subtilis*, with inhibition zone diameters of 24.0 mm for both **CoL1$_2$** and **CoL3$_2$**.

Conclusions

In this paper, we present a mechanochemical one-pot synthesis strategy that integrates the condensation covalent reaction of ammonia with aldehyde, metal coordination reactions, and dehydrohalogenation reactions. The raw materials employed include adamantylamine, 5-halosalicylaldehyde, and CoCl$_2$·6H$_2$O. Under the influence of mechanical forces, these reactions facilitate the self-ordering of the initial building blocks through synergistic interactions, leading to complex chemical processes that ultimately induce self-classification and ultra-high selective coordination. This method successfully yielded 12 Co(II) complexes with Schiff bases, including the κ^1-O-monodentate complex **CoCl$_2$(HL)$_2$** and the κ^2-O, N-bidentate complex **CoL$_2$**. Furthermore, this one-pot mechanochemical reaction not only simplifies the preparation procedure for Schiff base complexes but also enhances the complexity of mechanochemical multicomponent reactions. Notably, the reaction reached full conversion within 10 minutes, effectively demonstrating the advantages of mechanochemistry in green and sustainable synthesis. Additionally, the dormant chemical reactivity of the reactants was activated by mechanical force, resulting in the successful preparation of κ^1-O-monodentate complexes, which are typically challenging to obtain *via* solution methods. The reversible solid-state transformations between two complexes were studied by dehydrohalogenation/hydrohalogenation processes. The dehydrochlorination reaction from the complex **CoCl$_2$(HL)$_2$** to the complex **CoL$_2$** involves the cleavage of the N–H and Co–Cl bonds of the complex **CoCl$_2$(HL)$_2$** and the formation of the coordination bonds Co–N of the **CoL$_2$**. Meanwhile, **CoL$_2$** can also transform back into the complex **CoCl$_2$(HL)$_2$** by the absorption of HCl *via* grinding. This work provides us a good example, showing reaction pathways in one-pot synthesis and solid-state transformation by the understanding of mechanochemistry as a green route for the synthesis of Schiff base complexes.

Experimental

Materials and methods

All chemicals were obtained from commercial sources and used without further purification. Powder X-ray diffraction was performed with a Bruker D8 diffractometer ($\lambda = 1.54056$ Å). Single

crystal X-ray diffraction was carried out using a Bruker D8 QUEST X-ray single-crystal diffractometer. IR spectra were obtained with a PerkinElmer 100 FT-IR spectrometer using KBr pellets.

Mechanochemical synthesis of complexes $CoCl_2(HL)_2$ (L = L1–L6)

"One-pot" synthesis of $CoCl_2(HL1)_2$. Amantadine (1 mmol, 0.151 g), 5-chlorosalicylaldehyde (1 mmol, 0.156 g) and $CoCl_2$·$6H_2O$ (0.5 mmol, 0.119 g) in 2 : 2 : 1 molar ratio were ground in an agate mortar for 10 minutes, giving rise to a green powder, yield: 0.7105 g, 85%; m.p. 239.5–240.3 °C. IR (KBr): 3427 (m), 2906 (s), 2852 (m), 1643 (s), 1602 (w), 1526 (s), 1483 (s), 1324 (w), 1303 (m), 1229 (m), 1169 (s), 1112 (w), 1078 (m), 1032 (w), 833 (w), 793 (w), 682 (w), 627 (m), 521 (w), 492 (m), 446 (w). HRMS (ESI):m/z calculated for $C_{34}H_{40}Cl_4CoN_2O_2$ + H: 708.1176, [M + H$^+$] found: 708.1248.

"One-pot" synthesis of $CoCl_2(HL2)_2$. Amantadine (1 mmol, 0.151 g), 5-bromosalicylaldehyde (1 mmol, 0.210 g) and $CoCl_2$·$6H_2O$ (0.5 mmol, 0.119 g) in 2 : 2 : 1 molar ratio were ground in an agate mortar for 10 minutes, giving rise to a green powder, yield: 0.7105 g, 89%; m.p. 242.2–243.1 °C. IR (KBr): 3430 (m), 2048 (w), 2915 (s), 2853 (m), 2845 (m), 1641 (s), 1601 (m), 1529 (s), 1484 (s), 1454 (w), 1305 (m), 1233 (m), 1231 (m), 1171 (m), 1112 (m), 1079 (m), 940 (w), 834 (w), 794 (w), 683 (w), 628 (m), 523 (w), 495 (m), 447 (w). HRMS (ESI):m/z calculated for $C_{34}H_{40}Br_2Cl_2CoN_2O_2$ + Na: 783.5636, [M + Na] found: 783.0369.

"One-pot" synthesis of $CoCl_2(HL3)_2$. Memantine (1 mmol, 0.216 g), 5-chlorosalicylaldehyde (1 mmol, 0.156 g) and $CoCl_2$·$6H_2O$ (0.5 mmol, 0.119 g) in 2 : 2 : 1 molar ratio were ground in an agate mortar for 10 minutes, giving rise to a green powder, yield: 0.7105 g, 89%; m.p. 137.8–138.3 °C. IR (KBr): 3426 (m), 2917 (s), 2863 (w), 2845 (m), 2312 (w), 1643 (s), 1605 (s), 1531 (s), 1490 (s), 1455 (s), 1387 (s), 1301 (m), 1255 (w), 1231 (m), 1166 (s), 1024 (w), 937 (w), 870 (w), 825 (m), 799 (w), 735 (w), 644 (w), 585 (w), 541 (w). HRMS (ESI):m/z calculated for $C_{38}H_{48}Cl_4CoN_2O_2$+H: 764.1802, [M + H$^+$] found: 764.1874.

"One-pot" synthesis of $CoCl_2(HL4)_2$. Memantine (1 mmol, 0.216 g), 5-bromosalicylaldehyde (1 mmol, 0.2101 g) and $CoCl_2$·$6H_2O$ (0.5 mmol, 0.119 g) in 2 : 2 : 1 molar ratio were ground in an agate mortar for 10 minutes, giving rise to a green powder, yield: 0.7105 g, 87%; m.p. 119.2–119.8 °C. IR (KBr): 3436 (s), 2944 (w), 2915 (s), 2863 (w), 2844 (w), 2300 (w), 1642 (s), 1602 (m), 1528 (s), 1486 (s), 1455 (w), 1386 (m), 1302 (s), 1255 (w), 1231 (m), 1165 (s), 1023 (w), 868 (w), 823 (m), 798 (w), 721 (w), 629 (w), 516 (w). HRMS (ESI):m/z calculated for $C_{38}H_{48}Br_2Cl_2CoN_2O_2$ + Na: 874.0792, [M + Na] found: 874.0683.

"One-pot" synthesis of $CoCl_2(HL5)_2$. Rimantadine (1 mmol, 0.181 g), 5-chlorosalicylaldehyde (1 mmol, 0.156 g) and $CoCl_2$·$6H_2O$ (0.5 mmol, 0.119 g) in 2 : 2 : 1 molar ratio were ground in an agate mortar for 10 minutes, giving rise to a green powder, yield: 0.7105 g, 89%; m.p. 159.8–160.4 °C. IR (KBr): 3427 (m), 2905 (s), 2849 (m), 1647 (s), 1605 (w), 1529 (s), 1483 (s), 1386 (w), 1315 (m), 1283 (w), 1234 (m), 1173 (m), 1149 (w), 1089 (w), 1007 (s), 1034 (w), 871 (w), 826 (m), 798 (m), 714 (w), 689 (w), 637 (w), 547 (w). HRMS (ESI):m/z calculated for $C_{38}H_{48}Cl_4CoN_2O_2$ + H: 764.1802, [M + H$^+$] found: 764.1877.

"One-pot" synthesis of $CoCl_2(HL6)_2$. Rimantadine (1 mmol, 0.181 g), 5-bromosalicylaldehyde (1 mmol, 0.210 g) and $CoCl_2$·$6H_2O$ (0.5 mmol, 0.119 g) in 2 : 2 : 1 molar ratio were ground in an agate mortar for 10 minutes, giving rise to a green powder, yield: 0.7105 g, 89%; m.p. 167.9–168.4 °C. IR (KBr): 3444 (m), 2917 (s), 2863 (w), 2845 (m), 2312 (w), 1643 (s), 1605 (m), 1531 (s), 1489 (s), 1455 (s), 1388 (m), 1301 (m), 1255 (w), 1231 (m), 1166 (s), 1024 (w), 937 (w), 870 (w), 825 (m), 799 (w), 735 (w), 644 (w), 585 (w), 541 (w). HRMS (ESI):m/z calculated for $C_{38}H_{48}Br_2Cl_2CoN_2O_2$ + Na: 874.0792, [M + Na] found: 874.0672.

Mechanochemical synthesis of complexes CoL_2 (L = L1–L6)

"One-pot" synthesis of $CoL1_2$. Amantadine (1 mmol, 0.1513 g), 5-chlorosalicylaldehyde (1 mmol, 0.156 g), $CoCl_2$·$6H_2O$ (0.5 mmol, 0.119 g) and NaOH (1 mmol, 0.040 g) in 2 : 2 : 1 : 2 molar ratio were ground in an agate mortar aided by methanol (60 μL) for 5 minutes, yielding a red powder, yield: 0.6311 g, 88%, m.p. 290 °C. IR (KBr): 3434(m), 2908(s), 2850(m), 1598(s), 1522(s), 1455(s), 1389(s), 1347(w), 1315(m), 1268(w), 1243(w), 1166(m), 1132(w), 1107(m), 1077(m), 984(w), 934(w), 871(w), 823(m), 783(w), 753(m), 694(m), 662(m), 609(w), 548(m), 505(m), 452(w), 425(w). HRMS (ESI):m/z calculated for $C_{34}H_{38}Cl_2CoN_2O_2$ + K: 674.2355, [M + K] found: 674.1273.

"One-pot" synthesis of $CoL2_2$. Amantadine (1 mmol, 0.151 g), 5-bromosalicylaldehyde (1 mmol, 0.210 g), $CoCl_2$·$6H_2O$ (0.5 mmol, 0.119 g) and NaOH (1 mmol, 0.040 g) in 2 : 2 : 1 : 2 molar ratio were ground in an agate mortar aided by methanol (60 μL) for 5 minutes, yielding a red powder, yield: 0.6311 g, 89%, m.p. > 300 °C. IR (KBr): 3374(m), 3043(w), 2908(s), 2849(m), 1598(s), 1518(s), 1456(s), 1387(s), 1339(w), 1314(s), 1268(w), 1244(w), 1167(m), 1133(w), 1106(w), 1077(m), 985(w), 931(w), 872(w), 823(m), 781(w), 745(m), 685(w), 649(m), 605(w), 547(m), 499(m), 451(m), 424(w). HRMS (ESI):m/z calculated for $C_{34}H_{38}Br_2CoN_2O_2$ + K: 762.1570, [M + K] found: 762.0263.

"One-pot" synthesis of $CoL3_2$. Memantine (1 mmol, 0.216 g), 5-chlorosalicylaldehyde (1 mmol, 0.156 g), $CoCl_2$·$6H_2O$ (0.5 mmol, 0.119 g) and NaOH (1 mmol, 0.040 g) in 2 : 2 : 1 : 2 molar ratio were ground in an agate mortar aided by methanol (60 μL) for 5 minutes, yielding a red powder, yield: 0.6311 g, 86%, m.p. 236.7–238.4 °C. IR (KBr): 2909(m), 2863(w), 2846(m), 1601(s), 1523(s), 1456(s), 1411(w), 1387(s), 1316(m), 1297(w), 1254(w), 1166(s), 1132(w), 1093(w), 1055(w), 1026(w), 827(m), 809(w), 790(w), 734(w), 681(w), 663(w), 542(w), 514(w), 500(w). HRMS (ESI):m/z calculated for $C_{38}H_{46}Cl_2CoN_2O_2$ + H: 692.2268, [M + H] found: 692.2341.

"One-pot" synthesis of $CoL4_2$. Memantine (1 mmol, 0.216 g), 5-bromosalicylaldehyde (1 mmol, 0.210 g), $CoCl_2$·$6H_2O$ (0.5 mmol, 0.119 g) and NaOH (1 mmol, 0.040 g) in 2 : 2 : 1 : 2 molar ratio were ground in an agate mortar aided by methanol (60 μL) for 5 minutes, yielding a red powder, yield: 0.6311 g, 87%, m.p. 261.4–262.5 °C. IR (KBr): 2913(s), 1598(m), 1455(s), 1249(w), 1164(m), 1057(m), 1025(m), 985(w), 933(w), 824(m), 787(w), 648(w), 546(w), 505(w). HRMS (ESI):m/z calculated for $C_{38}H_{46}Br_2CoN_2O_2$ + H: 780.1258, [M + H] found:780.1331.

"One-pot" synthesis of $CoL5_2$. Rimantadine (1 mmol, 0.181 g), 5-chlorosalicylaldehyde (1 mmol, 0.156 g), $CoCl_2$·$6H_2O$

(0.5 mmol, 0.119 g) and NaOH (1 mmol, 0.040 g) in 2 : 2 : 1 : 2 molar ratio were ground in an agate mortar aided by methanol (60 μL) for 5 minutes, yielding a red powder, yield: 0.6311 g, 86%, m.p. 258.3–260.7 °C. IR 3438(m), 2899(s), 2847(m), 1600(s), 1520(m), 1453(s), 1391(s), 1314(m), 1169(m), 1083(m), 979(w), 870(w), 815(w), 708(m), 657(w), 498(m), 456(m). HRMS (ESI):m/z calculated for $C_{38}H_{46}Cl_2CoN_2O_2$ + H: 692.2268, [M + H] found: 692.2341.

"One-pot" synthesis of CoL6₂. Rimantadine (1 mmol, 0.181 g), 5-bromosalicylaldehyde (1 mmol, 0.210 g), $CoCl_2 \cdot 6H_2O$ (0.5 mmol, 0.119 g) and NaOH (1 mmol, 0.040 g) in 2 : 2 : 1 : 2 molar ratio were ground in an agate mortar aided by methanol (60 μL) for 5 minutes, yielding a red powder, yield: 0.6311 g, 89%, m.p. 264.3–265.6 °C. IR 3428(m), 2902(s), 2847(m), 1599(s), 1518(m), 1455(s), 1391(s), 1310(m), 1170(m), 1133(w), 1080(w), 975(w), 871(w), 824(w), 799(w), 684(m), 648(m), 496(m), 460(m). HRMS (ESI):m/z calculated for $C_{38}H_{46}Br_2CoN_2O_2$ + H: 780.1258, [M + H] found:780.1331.

Crystallization of CoCl₂(HL)₂ and CoL₂ (L = L1–L6)

Recrystallization of the six κ^1-*O*-monodentate complexes **CoCl₂(HL)₂** was carried out by evaporation of the above ground green products under ambient conditions using a variety of different solvents such as ethanol, acetone, dichloromethane, tetrahydrofuran, *N*,*N*-dimethylformamide, and dimethyl sulfoxide, but only acetonitrile (CH_3CN) gave rise to block-shaped single green crystals suitable for single crystal X-ray (SC-XRD) analysis, in about 2 days.

Recrystallization of **CoL2₂** was carried out by evaporation of the ground red product in methanol/dimethyl sulfoxide (DMSO) (10 : 1) solution, which gave rise to block-shaped red single crystals suitable for SC-XRD analysis, in about 7 days.

Recrystallization of **CoL3₂, CoL5₂** and **CoL6₂** was achieved through the evaporation of the ground red product in an ethyl alcohol solution, resulting in the formation of block-shaped red single crystals suitable for single crystal X-ray diffraction (SC-XRD) analysis within approximately 5 days.

Crystallography: single-crystal X-ray diffraction measurements of the crystals were performed with a Bruker Smart D8 Quest diffractometer equipped with a graphite monochromator. The determination of the unit-cell parameters and the data collection were performed with Mo-Kα radiation (λ = 0.71073 Å). The unit-cell parameters were obtained through least-squares refinements, and the structures were determined by direct methods and refined (on F^2 with all independent data) by the full-matrix least square method (SHELXTL 2014). Data were reduced by using the Bruker SAINT software. All the non-hydrogen atoms were directly located from different Fourier maps and refined with an isotropic displacement parameter. The hydrogen atoms in the ligand molecules were located in a difference electron density map and their positions were refined together with individual isotropic temperature factors.

Antibacterial activity experiment

The filter paper method was used to examine the antimicrobial activity against two Gram-positive (*Staphylococcus aureus* and *Bacillus subtilis*) and one Gram negative bacteria (*Escherichia coli*). The three activated bacteria were diluted to 10^{-6} CFU mL^{-1}; 100 μL of the bacterial solution was uniformly coated on the inactivated agar plate. Filter papers (6 mm) were immersed with HL, **CoCl₂(HL)₂** and **CoL₂** or the control group (cosolvent, *N*,*N*-dimethylformamide) and were transferred to the beef extract peptone AGAR medium agar plate. Thereafter, the agar plates were incubated at 37 °C for 48 h, the visible transparent halos on the plates were considered as the inhibition zones. The diameters and areas of the microbe-static ring were measured with a Vernier calliper. Each experiment was carried out in triplicate.

Author contributions

The manuscript was written through contributions of all authors. All authors have given approval to the final version of the manuscript.

Conflicts of interest

The authors declare no competing financial interest.

Data availability

Acknowledgements

References

1 X. Liu, Y. Li, L. Zeng, X. Li, N. Chen, S. Bai, H. He, Q. Wang and C. Zhang, *Adv. Mater.*, 2022, **34**, 2108327.

2 N. Fantozzi, J.-N. Volle, A. Porcheddu, D. Virieux, F. García and E. Colacino, *Chem. Soc. Rev.*, 2023, **52**, 6680–6714.

3 A. Krusenbaum, S. Grätz, G. T. Tigineh, L. Borchardt and J. G. Kim, *Chem. Soc. Rev.*, 2022, **51**, 2873–2905.

4 V. Martinez, T. Stolar, B. Karadeniz, I. Brekalo and K. Užarević, *Nat. Rev. Chem.*, 2023, **7**, 51–65.

5 D. Tan and F. García, *Chem. Soc. Rev.*, 2019, **48**, 2274–2292.

6 B. R. Naidu, T. Sruthi, R. Mitty and K. Venkateswarlu, *Green Chem.*, 2023, **25**, 6120–6148.

7 L. E. Wenger and T. P. Hanusa, *Chem. Commun.*, 2023, **59**, 14210–14222.

8 J. Zhang, L. Xu and W.-Y. Wong, *Coord. Chem. Rev.*, 2018, **355**, 180–198.

9 M. Kumar, A. K. Singh, V. K. Singh, R. K. Yadav, A. P. Singh and S. Singh, *Coord. Chem. Rev.*, 2024, **505**, 215663.

10 A. Abd-El-Aziz, Z. Li, X. Zhang, S. Elnagdy, M. S. Mansour, A. ElSherif, N. Ma and A. S. Abd-El-Aziz, *Top. Curr. Chem.*, 2025, **383**, 8.

11 I. Cocosila, A. Solé-Daura, P. Gotico, J. Forte, Y. Li and M. Fontecave, *ACS Catal.*, 2024, **14**, 9618–9627.

12 S. Khan, X. Chen, A. Almahri, E. S. Allehyani, F. A. Alhumaydhi, M. M. Ibrahim and S. Ali, *J. Environ. Chem. Eng.*, 2021, **9**, 106381.

13 X. Liu and J.-R. Hamon, *Coord. Chem. Rev.*, 2019, **389**, 94–118.

14 Y. Chen, H. Tang, H. Chen and H. Li, *Acc. Chem. Res.*, 2023, **56**, 2838–2850.

15 W. Ma, Y. Liu, N. Yu and K. Yan, *ACS Sustain. Chem. Eng.*, 2021, **9**, 16092–16102.

16 V. K. Singh, A. Chamberlain-Clay, H. C. Ong, F. León, G. Hum, M. Y. Par, P. Daley-Dee and F. García, *ACS Sustain. Chem. Eng.*, 2021, **9**, 1152–1160.

17 S. Zuo, S. Zheng, J. Liu and A. Zuo, *Beilstein J. Org. Chem.*, 2022, **18**, 1860–5397.

18 Y. Gui, X. Yao, I. A. Guzei, M. M. Aristov, J. Yu and L. Yu, *Chem. Mater.*, 2020, **32**, 7754–7765.

19 J.-F. Ayme and J.-M. Lehn, *Chem. Sci.*, 2020, **11**, 1114–1121.

20 L. Liang, W. Zhao, X.-J. Yang and B. Wu, *Acc. Chem. Res.*, 2022, **55**, 3218–3229.

21 J. Martí-Rujas and F. Guo, *Dalton Trans.*, 2021, **50**, 11665–11680.

22 S. Yang, Y. Yuan, X. Wang, Z. Hu and D. Guo, *J. Lumin.*, 2022, **242**, 118560.

23 A. A. Ahangar, A. A. Malik, I. Ahmad and A. A. Dar, *Dyes Pigm.*, 2023, **220**, 111742.

24 S. A. Boer, E. M. Foyle, C. M. Thomas and N. G. White, *Chem. Soc. Rev.*, 2019, **48**, 2596–2614.

25 G. Hubsher, M. Haider and M. S. Okun, *Neurology*, 2012, **78**, 1096–1099.

26 B. Kumar, K. Asha, M. Khanna, L. Ronsard, C. A. Meseko and M. Sanicas, *Arch. Virol.*, 2018, **163**, 831–844.

27 H. D. Mai, N. M. Tran and H. Yoo, *Coord. Chem. Rev.*, 2019, **387**, 180–198.

28 G. Peng, Y. Chen, B. Li, Y.-Q. Zhang and X.-M. Ren, *Dalton Trans.*, 2020, **49**, 5798–5802.

29 C. Xu, L. Xiao-Chen, J. Xu-Dong, Y. Qi, H. Guang-Chao, G. Yu-Chen and H.-H. Hu, *J. Coord. Chem.*, 2014, **67**, 352–362.

30 M. V. Novozhilova, E. A. Smirnova, J. A. Polozhentseva, J. A. Danilova, I. A. Chepurnaya, M. P. Karushev, V. V. Malev and A. M. Timonov, *Electrochim. Acta*, 2018, **282**, 105–115.

31 N. Singh, P. Kumar, S. Ahmad, J. Gupta, K. Raza and A. A. Hashmi, *J. Mol. Struct.*, 2025, **1321**, 139874.

32 T. E. Shaw, J. Arami, J.-F. Ayme, J.-M. Lehn and T. Jurca, *RSC Mechanochem.*, 2024, **1**, 33–37.

33 H. Chen, Z. Guo, D. Feng, X. Jin and F. Guo, CCDC 2083179: Experimental Crystal Structure Determination, 2025, DOI: **10.5517/ccdc.csd.cc27xqb7**.

34 H. Chen, Z. Guo, D. Feng, X. Jin and F. Guo, CCDC 2083171: Experimental Crystal Structure Determination, 2025, DOI: **10.5517/ccdc.csd.cc27xq2z**.

35 H. Chen, Z. Guo, D. Feng, X. Jin and F. Guo, CCDC 2343391: Experimental Crystal Structure Determination, 2025, DOI: **10.5517/ccdc.csd.cc2jnh8z**.

36 H. Chen, Z. Guo, D. Feng, X. Jin and F. Guo, CCDC 2257072: Experimental Crystal Structure Determination, 2025, DOI: **10.5517/ccdc.csd.cc2frnsn**.

37 H. Chen, Z. Guo, D. Feng, X. Jin and F. Guo, CCDC 2121576: Experimental Crystal Structure Determination, 2025, DOI: **10.5517/ccdc.csd.cc296ny4**.

38 H. Chen, Z. Guo, D. Feng, X. Jin and F. Guo, CCDC 2257071: Experimental Crystal Structure Determination, 2025, DOI: **10.5517/ccdc.csd.cc2frnrm**.

39 H. Chen, Z. Guo, D. Feng, X. Jin and F. Guo, CCDC 2074209: Experimental Crystal Structure Determination, 2025, DOI: **10.5517/ccdc.csd.cc27mcz7**.

40 H. Chen, Z. Guo, D. Feng, X. Jin and F. Guo, CCDC 2343393: Experimental Crystal Structure Determination, 2025, DOI: **10.5517/ccdc.csd.cc2jnhb1**.